European Rotorcraft Forum

ROTOR CONTROL EQUIVALENT TURBULENCE INPUT (RCETI) MODELS

Mahmoud A. Hayajnh mhayajnh3@gatech.edu

J.V.R. Prasad jvr.prasad@ae.gatech.edu

School of Aerospace Engineering
Georgia Institute of Technology
Atlanta, Georgia, USA

Abstract

This paper presents a first step toward the generalization of the hover/low-speed Control Equivalent Turbulence Inputs (CETI) models for different helicopter configurations. The rotor hub-loads are used as the outputs to which the turbulence-related spectra are matched in order to achieve this. Furthermore, the rotor swash-plate deflections are considered as inputs to create what is referred to herein as the Rotor Control Equivalent Turbulence Inputs (RCETI) model. Development of an RCETI model, that provides rotor loads spectra similar to those produced by vertical turbulence, is carried out using a representative model of the UH-60 helicopter in FLIGHTLAB®. The effect of altering the rotor parameters on the RCETI model is studied and presented in the paper.

NOMENCLATURE

C_T	Thrust coefficeint
C_W	Weight coefficient
J	Fit cost function
L_w	Vertical turbulence scale length, ft
N_b	Number of rotor blades
R	Rotor radius, ft
S_x	Power Spectral Density PSD of signal x, $dB = 10log10(x)$
U_0	Mean wind speed, ft/s
V_{ZB}	Body z-axis component of velocity, ft/s
δ_c	Pilot collective input, percent
ω	Frequency, rad/s
σ	Rotor solidity ($\frac{N_b c}{\pi R}$)
σ_w	Vertical turbulence intensity, ft/s
θ_0	Swash-plate collective angle, degree
c	Blade chord length, ft
s	Laplace variable
w_z	Turbulence vertical velocity, ft/s
G	Transfer function gain, $dB = 20log10(\|G\|)$
U	Input
Y	Output
n	White noise source

1. INTRODUCTION

Turbulence modeling is essential for assessing the ability of an aircraft to perform certain tasks in adverse weather conditions. In addition, accurate turbulence models are needed for the design and evaluation of disturbance rejection controllers in simulation. Moreover, the highly nonlinear spatial variation of air wakes in the vicinity of buildings, ships, and other obstacles during nap-of-the-earth flight for a range of vertical lift platforms causes significant control and potential safety issues, especially

during take-off and landing. These scenarios require vehicles and their control systems be designed with effective gust rejection features for safe operations in these highly complex flow environments.

The traditional approach to model turbulence for fixed-wing aircraft is done by assuming that the aircraft velocity is much higher than the turbulence velocity, and thus, a spatially frozen-field pattern of body axis gust velocities is generated from, for example, Von Karman or Dryden turbulence models[1] and are summed into the aircraft equations of motion. Although an improved approach by the implementation of complex rotating frame turbulence models[2] was found to be applicable for low speed/hover tasks, such approach is computationally expensive and can be difficult to implement in real-time simulations[3].

The notion of using control inputs that result in vehicle response that is stochastically similar to its response to atmospheric turbulence has been identified to reduce in situ flight testing, thus reducing risk during vehicle and its control system design. This different approach was first put forward by the National Research Council (NCR), Canada[4]. The angular rates and vertical accelerations from data of the Bell 205 hovering in turbulence were processed via a first-order inverse model of the aircraft to obtain input traces. These traces were then used as inputs to the aircraft actuators, yielding a response similar to the one measured from flight in turbulence. This notion was later extensively studied by the US Army Aeroflightdynamics Directorate (AFDD) at NASA Ames, which resulted in the development of the Control Equivalent Turbulence Input (CETI) models. In the CETI approach, the control inputs required to drive the aircraft responses to become statistically consistent with responses in actual turbulence are determined. The CETI model for the UH-60 helicopter was developed using vehicle responses from flight tests in turbulence[5]. The method was later applied to the EC135 helicopter at the German Aerospace Center (DLR)[6], showing that the approach can be applied to different aircraft. These models, however, are developed for the specific vehicles from which the data are extracted. The lack of the existence of a CETI model that can be scaled for different vehicle configurations provides motivation for developing a RCETI model that can be scaled for different rotor configurations. This research builds on previous studies that developed turbulence models for specific helicopters, to develop an equivalent control input for the rotor by utilizing the hub loads as outputs to develop the Rotor Control Equivalent Turbulence Input (RCETI) models. This recognizes that rotors are the dominant aerodynamic load-producing components at hover and low speeds. This, subsequently, reduces the parameter space in the generalization of the RCETI modeling to rotor parameters only.

As such, the purpose of the present research is to develop a hover/low-speed RCETI model for a rotor operating in atmospheric turbulence which generates rotor control inputs that produce hub loads with a spectrum consistent with that produced due to turbulence and is assessed on different rotor parameters and configurations.

The paper is organized as follows: First, a description of the methodology to find the PSDs of the CETI traces in the frequency domain is presented. The method is carried out to find the traces of the inputs using aircraft rates and compared to the results with the use of rotor hub-loads. Subsequently, an RCETI model is developed and evaluated for different mean wind speeds and turbulence intensities. Lastly, the effect of altering the rotor parameters on the RCETI model is assessed and presented.

2. METHODOLOGY

The CETI model developed previously[5] used a combined frequency and time-domain approach. The measured aircraft rates were processed through a stabilized inverse of an identified aircraft model to generate the traces of the control inputs. The remnant input time histories, after subtracting the input traces from the expected control inputs, were analyzed in the frequency-domain to identify the CETI model parameters. This combined method requires the development of a stabilized inverse of the identified aircraft model to perform the inverse time-domain simulation. A similar approach was used in other studies[6,7].

Recently, a frequency-domain approach was proposed and used to develop the CETI model[8,9], which did not require an inverse aircraft model. This approach is considered in the following discussion and the methodology for a Single Input Single Output (SISO) system is described.

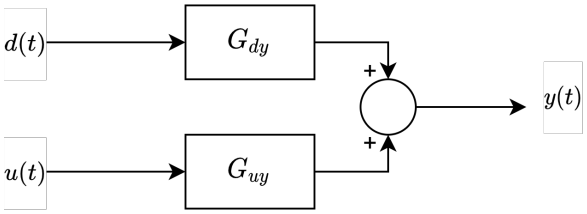

Figure 1: Vehicle response to both input and turbulence

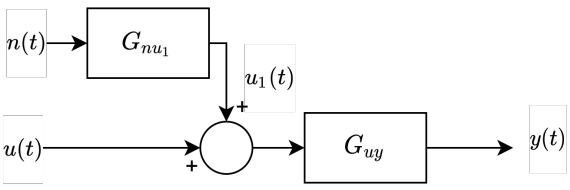

Figure 2: Block diagram of control equivalent turbulence input model.

Consider the block diagram shown in Fig. 1, the SISO equation for this diagram can be written in the frequency domain as:

$$Y(\omega) = G_{uy}(\omega)U(\omega) + G_{dy}(\omega)D(\omega) \quad (1)$$

where G_{uy} represents the aircraft response to input u, and G_{dy} represents the aircraft response to turbulence d.
The equation for the system with the block diagram in Fig. 2 is:

$$Y(\omega) = G_{uy}(\omega)[U(\omega) + U_1(\omega)] \quad (2)$$

where U_1 represents the remnant input that is used to account for the aircraft response to turbulence. By rearranging Eq. (2), to solve for the remnant input U_1:

$$U_1(\omega) = \frac{1}{G_{uy}(\omega)}Y(\omega) - U(\omega) \quad (3)$$

The power spectral density (PSD) of the remnant input ($S_{u_1u_1}$) is defined as follows[10]:

$$S_{u_1u_1}(\omega) = \lim_{T\to\infty} \frac{1}{T}\{U_1^* U_1\} \quad (4)$$

And the magnitude of the CETI transfer function model G_{nu_1} is then found when driven by a unity PSD white noise input as:

$$|G_{nu_1}| = \sqrt{S_{u_1u_1}} \quad (5)$$

A CETI transfer function can then be identified via frequency domain system identification techniques such as CIFER®[11].
As has been noted in the introduction, the spectra of the aircraft rates were the basis in earlier efforts to create the CETI models. In order to reduce the number of parameters for the generalization of the RCETI model, the fixed system hub-loads comprising rotor thrust, pitch moment, and roll moment may be considered. The stochastic characterization of vehicle response to turbulence is very largely driven by the stochastic characterization of rotor hub loads. Hence, the RCETI methodology is aimed at finding rotor control inputs that result in hub loads stochastically similar to those due to atmospheric turbulence.
For example, the spectrum of the thrust coefficient (C_T) as output due to turbulence is found using linear time-invariant models developed from FLIGHTLAB®[12], where the z-axis wind velocity is considered as input, this can be found as follows:

$$S_{C_T}(\omega) = |\frac{C_T}{w_z}(\omega)|^2 S_{w_z}(\omega) \quad (6)$$

where $S_{w_z}(\omega)$ is the spectrum of the turbulence.
Next, an inverse mapping of the load spectrum to rotor control spectrum comprising collective (θ_0) control is developed. This can be found in the frequency domain by the following equation:

$$S_{\theta_0}(\omega) = |\frac{C_T}{\theta_0}(\omega)|^{-2} S_{C_T}(\omega) \quad (7)$$

At this point, the RCETI models are formed by converting the control spectrum to a parametric filter transfer function via frequency domain system identification techniques using CIFER®. In this first step towards the identification of RCETI models, only the vertical component of the turbulence with hub-fixed sampling (*i.e.*, the full vehicle is subjected to the same turbulence velocity fluctuations) is considered. This, of course, is a simplifying assumption that will be replaced by the blade-element sampling approach in future work.

3. RESULTS

In the example presented herein, we consider the simple case of hub-fixed turbulence where the vehicle is subjected to fluctuations in the z-axis wind velocity. The PSD of turbulence in the z-axis is calculated using the Dryden turbulence model[1], where the Dryden turbulence transfer function for the vertical axis is given by:

$$\frac{w_z}{n} = \frac{\sigma_w \sqrt{\frac{U_0}{\pi L_w}}(\sqrt{3}s + \frac{U_0}{L_w})}{(s + \frac{U_0}{L_w})^2} \quad (8)$$

where s is the Laplace variable, n is a unity-power white noise source, σ_w is the turbulence intensity, U_0 is the mean wind speed, and L_w is the scale length which is set to (2R)[5], where R is the radius of the rotor.

3.1. FLIGHTLAB® non-linear model and Linear Time-Invariant approximations

The model utilized in this analysis is a high fidelity non-linear model that is representative of a UH-60 helicopter which is implemented in FLIGHTLAB®.

The model features finite-element blade representation and a 33-state Peters-He inflow model.
FLIGHTLAB® is utilized to construct linear time-periodic (LTP) models with the vehicle body z-axis component of velocity (V_{ZB}) as the output and the pilot collective (δ_c) and the z-axis wind velocity (w_z) as inputs. The states retained in this model includes body and rotor states, for a total of 90 states. The harmonic decomposition[13] is used to develop high-order LTI approximations to the LTP dynamics. Two approximations are developed for the LTP model. One is done with the zeroth harmonic states (*i.e.*, the averaged LTI with a total of 90 states) as done traditionally, while the other is done by retaining up to the fourth harmonic states (with a total of 810 states). To that end, we have the following transfer functions:

$$G_{\delta_c V_{ZB}} = \frac{V_{ZB}}{\delta_c} \tag{9}$$

$$G_{w_z V_{ZB}} = \frac{V_{ZB}}{w_z} \tag{10}$$

The transfer functions in Eq. (9) and Eq. (10) represent the transfer functions G_{uy} and G_{dy} in Fig. 1, respectively. A frequency sweep input is applied to the FLIGHTLAB® non-linear model in order to validate the LTI approximations. The frequency responses from CIFER® and from the LTI approximations are shown in Fig. 3, and Fig. 4. The frequency response of the high-order LTI matches well with the CIFER results, while there is a mismatch with the frequency response from the averaged LTI. It can be concluded that the use of the averaged LTI is not sufficient to represent the dynamics and there is a need for the high order LTI approximations (*i.e.*, up to the fourth harmonics).

3.2. Recovering input traces

The frequency range that is relevant to the pilot workload and manual control is about 1-10 rad/s[5,14]. To include this range, a frequency range of 1-20 rad/s is chosen for the analysis[5]. The PSD of the vehicle response ($S_{V_{ZB}}$) due to turbulence is found in the frequency domain directly from transfer functions. The Dryden model spectrum is used as the input to the transfer function in Eq. (10) and the resulting PSD of the vehicle response is shown in Fig. 5 (solid blue line). For this nominal case, the parameters for the Dryden model are chosen following one of the flight tests from Lusardi et al.[3] as follows: mean wind speed of 22 knots ($U_0 = 22$ knots), turbulence intensity of 5.5 ft/s ($\sigma_w = 5.5$ ft/s), and a scale length of 2R where R is the radius of the main

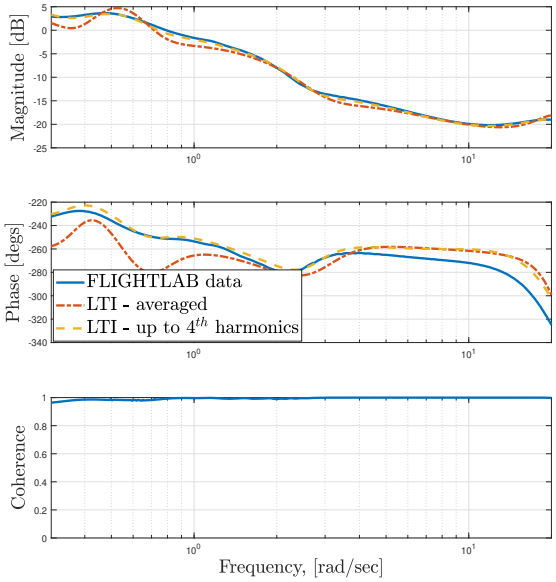

Figure 3: Frequency response of body z-axis velocity component to pilot collective input V_{ZB}/δ_c

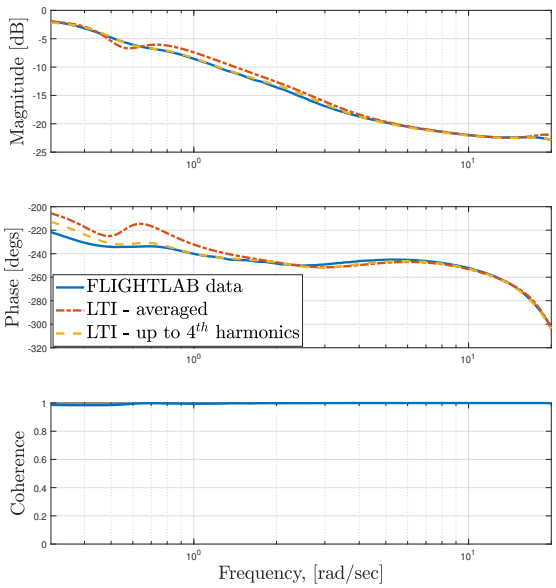

Figure 4: Frequency response of body z-axis velocity component to vertical gust V_{ZB}/w_z

rotor. The resulting PSD for the vertical speed is similar to the one found from the flight test data by Lusardi et al.[3] in similar flight conditions.
In the next step, the transfer function in Eq. (9) is used to find the input spectrum (S_{δ_c}) that would produce the same body z-axis velocity component spectrum produced by turbulence. The resulting in-

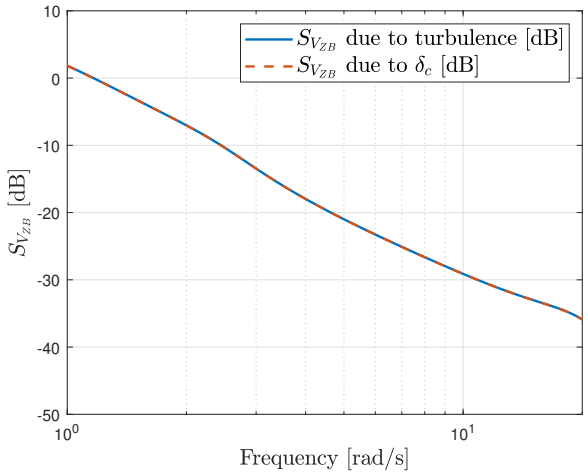

Figure 5: PSD of the body z-axis velocity component

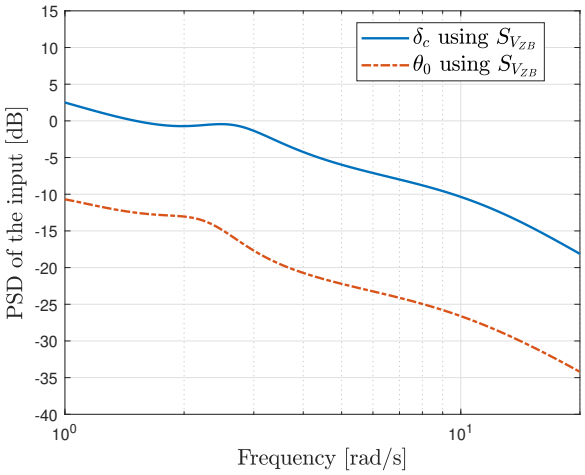

Figure 6: PSD of the remnant input required to produce the output spectrum due to turbulence (δ_c Vs. θ_0)

put spectrum which represents the CETI model is shown in Fig. 6 (solid blue line). To confirm the results, S_{δ_c} is used as input to the vehicle to find the body z-axis velocity component spectrum shown in Fig. 5 (dashed red line), which matches with the body z-axis velocity component spectrum due to turbulence. This step is similar to what has been done traditionally to develop the CETI models.

3.3. Pilot cyclic inputs Vs. swash-plate inputs

In this case, as a first step to developing the RCETI models, the swash-plate collective angle (θ_0) is considered instead of the pilot collective input (δ_c) as input in the transfer function G_{uy}. This leads to the transfer function:

$$(11)\quad G_{\theta_0 V_{ZB}} = \frac{V_{ZB}}{\theta_0}$$

The same analysis is done to find the input spectrum that would produce the same output spectrum due to turbulence. The result for the spectrum of θ_0 is shown in Fig. 6 (dashed red line). It is clear that the difference between the spectrum of δ_c and θ_0 is a scaling factor, as expected.

3.4. Vehicle Response Vs. hub-loads spectra due to turbulence

It is necessary to demonstrate that the turbulence effect can be captured by utilizing the hub-loads spectra rather than the vehicle rates spectra, which have been employed in previous studies. Figure 7 shows the PSD of both the vertical acceleration ($\dot{V}_{ZB}$) and the thrust coefficient (C_T) owing to turbulence input. Adding a factor of 75.7 dB to the thrust coefficient spectrum yields a spectrum that is close to the vertical acceleration spectrum. Since the vehicle is hovering in a turbulence field with a selected mean wind speed, this factor is proportional to the weight of the vehicle. This result supports the assumption that the rotor is the primary load-producing element in turbulence. This assumption was verified in earlier investigations[5,6] by exposing the vehicle to turbulence at various azimuthal angles and observing the similarities of the resultant PSDs of the vehicle rates.

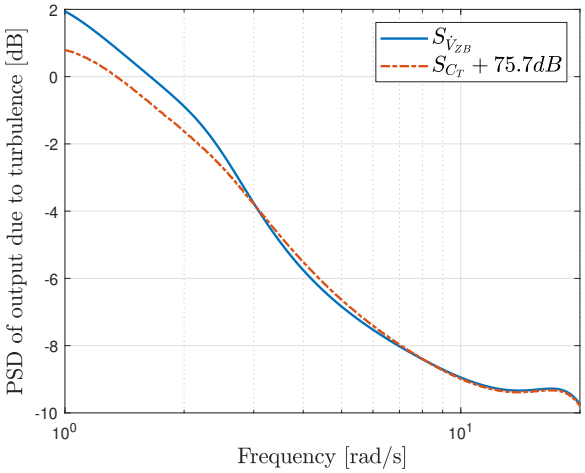

Figure 7: PSD of the outputs due to turbulence

3.5. Aircraft rates Vs. hub-loads as outputs

At this point, the thrust coefficient is used as the output of the transfer functions, that is, we try to match

the spectrum of the thrust coefficient due to turbulence by the use of the swash-plate collective angle as input. This yields what we refer to in this analysis as the RCETI model. The PSD of the RCETI model is shown in Fig. 8 (dashed red line) along with the PSD of the CETI model if the PSD of the body z-axis velocity component is matched.

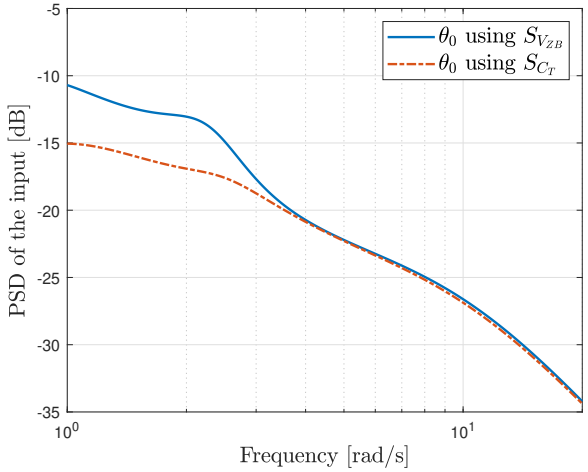

Figure 8: PSD of the remnant input required to produce the output spectrum due to turbulence using different outputs

The results in Fig. 8 show that, for frequencies higher than 3 rad/s, the PSDs of the input that is required to produce the body z-axis velocity component or the thrust coefficient match well. However, if the body z-axis velocity component is taken into account, the PSD of the input is larger at low frequencies. This discrepancy may be explained by the larger spectrum of $\dot{V}_{ZB}$, compared to ($C_T * ScaleFactor$), that results from the turbulence in this frequency range, which would need greater swash-plate angles (see Fig. 7). Additionally, when creating the LTI approximations, there might have been numerical errors that could contribute to this mismatch.

3.6. RCETI model with nominal rotor parameters

In this section, two steps are done to show the effect of the turbulence parameters on the developed CETI traces. First, the mean wind speed is fixed to 22 knots (*i.e.*, $U_0 = 22$ knots), while the turbulence intensity (σ_w) is changed from 3 ft/s to 6 ft/s with an increment of 1 ft/s. The PSDs of the RCETI are shown in Fig. 9 (solid lines), where it is clearly seen that the effect of the turbulence intensity is a gain difference in the RCETI model.
The second step is done by fixing the turbulence

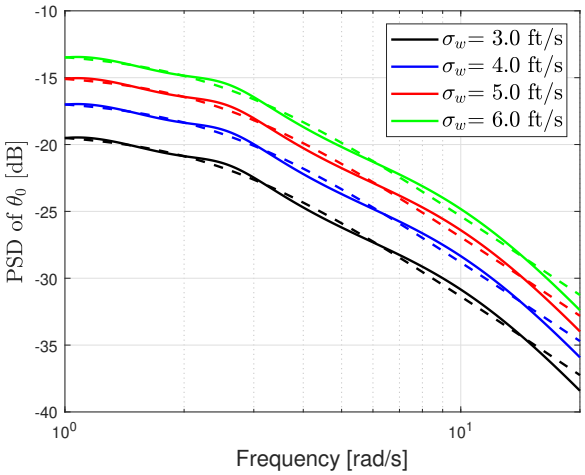

Figure 9: PSD of the remnant input for different turbulence intensity

intensity to 4.0 ft/s and changing the mean wind speed. For this analysis, different transfer functions were found for different mean wind speed conditions. The PSDs of θ_0 are shown in Fig. 10 for the different flight conditions (solid lines). The gain of the necessary input is seen to increase as the mean wind speed increases. Additionally, Figure 10 demonstrates that unlike the situation of modifying σ_w, the change in this instance is not only a gain in the RCETI model.

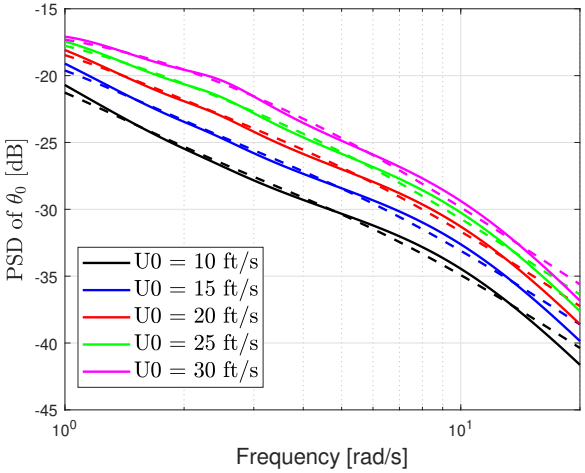

Figure 10: PSD of the remnant input for different mean wind speed

CIFER® is utilized to develop a white-noise-driven second-order filter for each of the cases (the dashed lines in Fig. 9 and Fig. 10). These transfer functions have the following form:

$$\frac{\theta_0}{n} = A\frac{(s + C_1(U_0/L_w))}{(s + C_2(U_0/L_w))(s + C_3(U_0/L_w))} \quad (12)$$

where,

$$A = K(\sigma_w)\sqrt{\frac{3U_0}{\pi L_w}} \quad (13)$$

and C_1, C_2 and C_3 are functions of the mean wind speed.
The function $K(\sigma_w)$ is found from the first test (*i.e.*, by fixing the mean wind speed (U_0) and changing the turbulence intensity (σ_w)). Table 1 summarizes the values of the different filter parameters along with the fit cost function J. The fit cost J for each case is well below $J \leq 50$, implying an excellent match to the PSD data[11]. Notice that the values of the other parameters are fixed to constant values since they are not functions of the turbulence intensity (σ_w). The function $K(\sigma_w)$ is found to be linear as follows:

$$K(\sigma_w) = 0.115\sigma_w \quad (14)$$

Table 1: Parameters of RCETI transfer functions when changing σ_w.

σ_w (ft/s)	A	$K(\sigma_w)$	C_1	C_2	C_3	J
3	0.28	0.34	2.4	2	2.8	10.3
4	0.37	0.46	2.5	2	2.8	10.3
5	0.47	0.58	2.4	2	2.8	10.3
6	0.56	0.69	2.5	2	2.8	10.3

Table 2 provides a summary of the parameters for the transfer functions as well as the fit cost function obtained from CIFER® for the case of changing the mean wind speed. The value for C_1 does not alter significantly for this case of vertical turbulence. Thus, this value is set to an approximate value of 2.5 in CIFER®. A good match to the PSD data is shown by the fit cost J for each case being well below $J \leq 50$[11]. Since the value of σ_w is set to 4.0 ft/s, it is noted that the value of $K(\sigma_w)$ is the same for all of the cases.

Table 2: Parameters of RCETI transfer functions when changing U_0.

U_0 (ft/s)	$K(\sigma_w)$	C_1	C_2	C_3	J
10	0.46	2.5	0.58	5.16	11.5
15	0.46	2.5	0.76	4.7	11.3
20	0.46	2.5	0.93	4.37	10.9
25	0.46	2.5	1.16	4.00	10.5
30	0.46	2.5	1.5	3.46	10.2

From the data in Table 2, the functions for C_2 and C_3 are found to be quadratic and are as follows:

$$C_2 = 4(U_0/L_w)^2 - 0.7(U_0/L_w) + 0.57 \quad (15)$$

$$C_3 = -5.5(U_0/L_w)^2 - 0.13(U_0/L_w) + 5.4 \quad (16)$$

To check the developed RCETI model, a case of U_0 = 16.5 ft/s and σ_w = 4.5 ft/s (which is not used in developing the model) is considered. Based on the developed RCETI model, the white-noise-driven filter can be found as:

$$\frac{\theta_0}{n} = 0.28\frac{(s+2.5)}{(s+0.74)(s+4.8)} \quad (17)$$

Both the Dryden vertical gust and the filter in Eq. (17) are used as inputs to the transfer functions to find the spectra of θ_0 and C_T. The results are shown in Fig. 11(a) and Fig. 11(b), where the RCETI model is shown to produce similar results to those of the vertical gust. The cost function J for θ_0 is found to be 11.1 which is well below $J \leq 50$. It is concluded that one can develop the RCETI model for helicopters by utilizing the rotor hub-loads as outputs and the rotor swashplate deflections as inputs.

3.7. Change of parameters

The parameters that are investigated in this study are as follows:

1. The vehicle weight coefficient (C_W).
2. The number of blades (N_b).
3. The blade chord length (c).

Changing the weight of the vehicle changes the thrust coefficient required for trim for the same flight condition. To assess how changing the vehicle weight impacts the RCETI model, the weight of the vehicle is altered in FLIGHTLAB® (the nominal value for C_W equals 0.006 and it is altered to 75% and 125% of the nominal value). Different Linear-Time Invariant approximations are developed and the same analysis is done to find the PSDs of the required inputs. In Fig. 12, the PSDs of the thrust coefficient for different values of the weight are shown. As expected, the PSDs of the thrust coefficient for different weight configurations are similar. Again, this is suggesting that altering the weight of the vehicle while maintaining the same rotor parameters will not have a significant impact on the rotor thrust coefficient variations due to turbulence.
Figure 13 shows the PSDs of the required input for different values of the vehicle weight. A slight mismatch between the PSDs at low frequencies may be the result of numerical errors made during vehicle trimming and during the development of the LTI approximations.
Next, the effect of changing the number of blades (N_b) of the rotor on the RCETI model is also considered here. To address this, transfer functions are

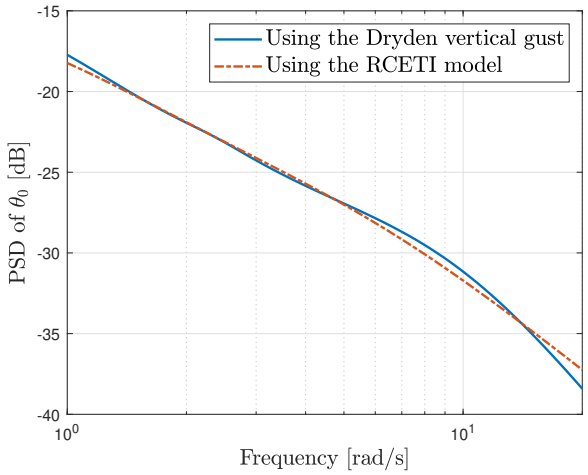

((a)) PSD of θ_0.

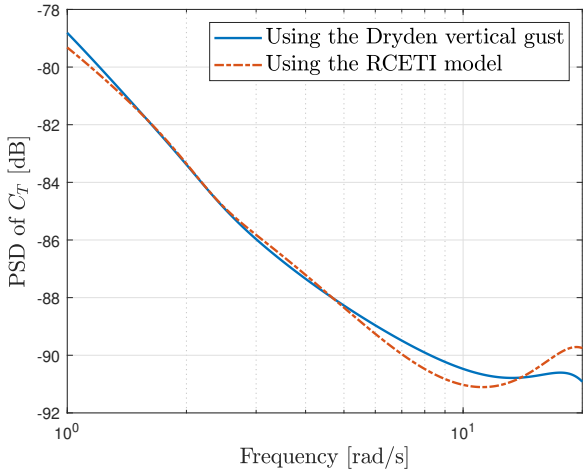

((b)) PSD of C_T.

Figure 11: Comparison between the results from Dryden turbulence and from RCETI model for $U_0 = 16.5$ ft/s and $\sigma_w = 4.5$ ft/s.

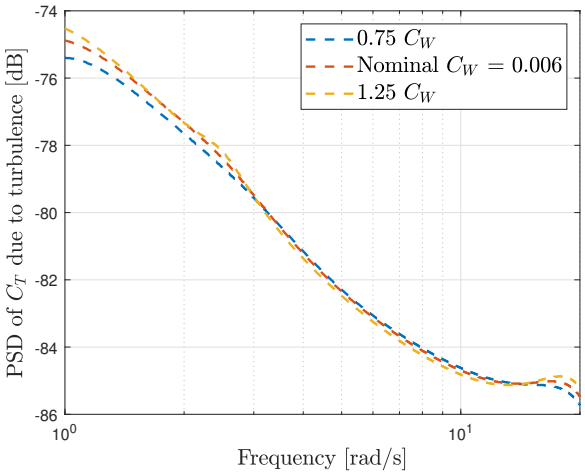

Figure 12: PSD of the thrust coefficient due to turbulence for different vehicle weight

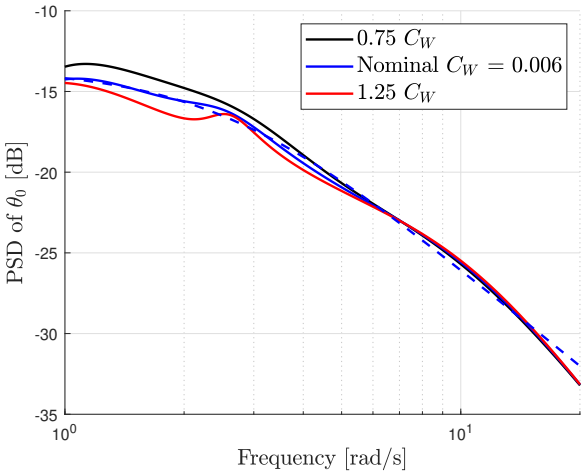

Figure 13: PSD of the remnant input for different vehicle weight

developed for the different numbers of blades of the rotor (*i.e.*, $N_b = 3, 4$, and 5). The PSDs of the thrust coefficient in Fig. 14 show that the spectrum of C_T increases with increasing the number of blades. This increase is anticipated since a larger area of the rotor is exposed to turbulence with more number of blades. However, this difference does not greatly alter the RCETI model since, in the case of more number of blades, the same deflection of the swashplate angle would create a higher spectrum for the thrust coefficient. Figure 15 illustrates this outcome by showing that the PSDs of the input are not greatly affected by changing the number of blades of the rotor.

In the last phase, the chord length of the blades is altered (from a nominal value for the UH-60 of 1.73 ft to 75% and 125% of the nominal value), and its impact on the RCETI model is observed. Since more surface area is exposed to turbulence when the chord length is larger, as is the case with more rotor blades, it is expected to observe higher spectra for the thrust coefficient, as seen in Fig. 16. Furthermore, as in the case of the different numbers of rotor blades, the PSD of the input does not change significantly, suggesting that the same RCETI model could be used to simulate the effect of vertical turbulence on rotor loads when changing the chord length of the rotor blades. Although the change of the chord length changes the rotor solidity (σ) by the same ratio as in the case of different numbers of rotor blades, the RCETI results from both cases are not the same. The reason for this could be that the order of the LTI approximations changes when changing the number of rotor blades (*i.e.*, different num-

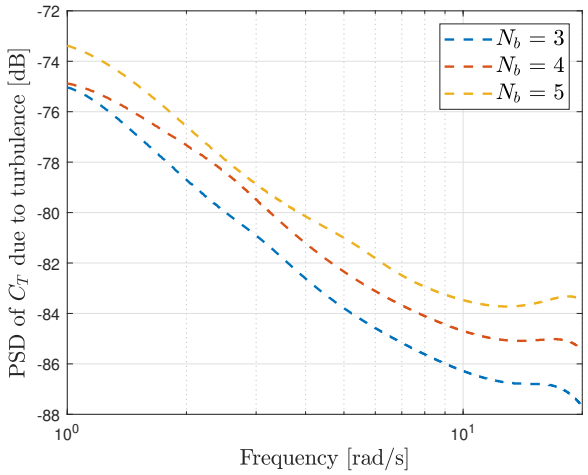

Figure 14: PSD of the thrust coefficient due to turbulence for different rotor number of blades

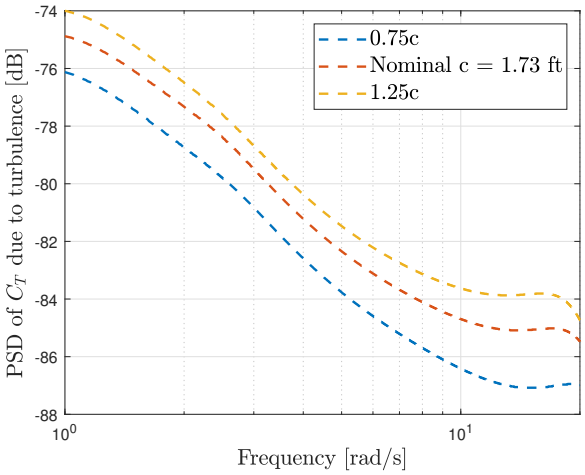

Figure 16: PSD of the thrust coefficient due to turbulence for different blade chord lengths

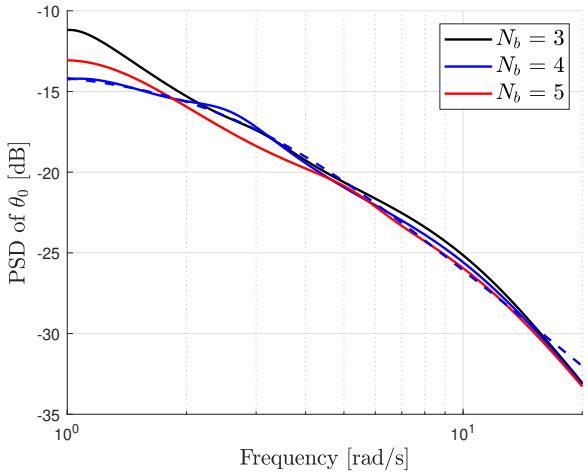

Figure 15: PSD of the remnant input for different rotor number of blades

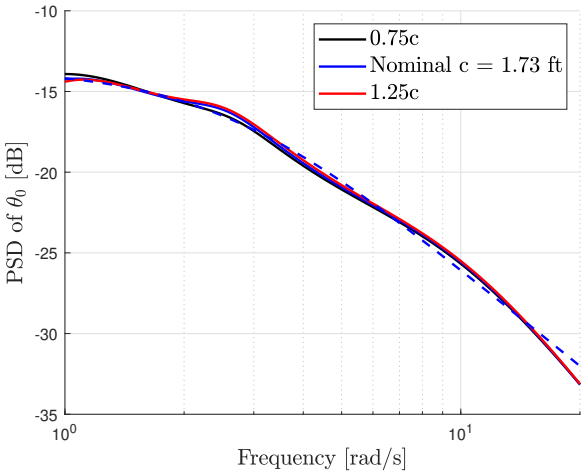

Figure 17: PSD of the remnant input for different blade chord lengths

ber of rotor states), while these LTI approximations have the same order when changing only the chord length. One needs to keep in mind that this analysis is done using the hub-fixed sampling case for turbulence. The results need not be the same if the blade-element sampling case is considered, which will be done in future work.

For each of the above instances, the cost function J is calculated using the same RCETI from the nominal example (the dashed lines in Figs. 13, 15, and 17) and can be found in Table 3. It is noted that the worst case is when changing the number of blades to 3. However, the value of $J = 32$ is still well within the acceptable range for the fit (*i.e.*, $J \leq 50$).

4. CONCLUDING REMARKS

In this work, the concept of Control Equivalent Turbulence Input was investigated for the rotors to develop the Rotor Control Equivalent Turbulence Input (RCETI) models. The vehicle's heave axis response was studied as a basic example and the RCETI model was developed using CIFER®. The effect of changing the rotor parameters on the RCETI model was studied as well. The following conclusions can be drawn from this work:

1. RCETI models can be created using the rotor swash-plate inputs to replicate the output spectrum caused by turbulence.

2. The rotor hub-loads can be employed as the outputs to which the spectrums are matched.

Table 3: The fit cost function J for the cases of changing the rotor parameters.

Case	The fit cost function J
Nominal parameters*	9.96
0.75 C_W	15.78
1.25 C_W	14.58
$N_b = 3$	32.4
$N_b = 5$	16.59
0.75 c	10.3
1.25 c	10.12

* ($C_W = 0.006$, $N_b = 4$, and $c = 1.73ft$)

3. For the simple case of hub-fixed sampled turbulence, the same RCETI model may be applied with varying rotor parameters such as the number of blades or the chord length.

Future work will include forming the RCETI model for the different rotor controls (*i.e.*, θ_0, θ_{1s}, and θ_{1c}) using spectrum of the hub-loads (*i.e.*, C_T, C_{M_y}, and C_{M_x}) (*i.e.*, the Multi-Input Multi-Output case). Furthermore, the blade-element sampling of the gust will be implemented as it represents a more realistic simulation of the turbulence. In addition, more rotor parameters that can affect the various rotor hub-loads will be investigated.

5. ACKNOWLEDGMENTS

This research was partially funded through the U.S. Army/Navy/NASA Vertical Lift Research Center of Excellence at Georgia Tech under the direction of Mahendra Bhagwat of the US Army Futures Comment, Agreement No. W911W6-21-2-0001. Opinions, interpretations, conclusions, and recommendations are those of the authors and are not necessarily endorsed by the United States Government.

REFERENCES

[1] Anon., "Flying qualities of piloted aircraft," *Dept. of Defense Interface Standard TR*, February 2006.

[2] G. Gaonkar, "Review of turbulence modeling and related applications to some problems of helicopter flight dynamics," *Journal of the American Helicopter Society*, vol. 53, pp. 87–107, 01 2008.

[3] J. Lusardi, C. Blanken, and M. Tischler, "Piloted evaluation of a uh60 mixer equivalent turbulence simulation model," 11 2002.

[4] S. W. Baillie and J. M. Morgan, "An in-flight investigation into the relationships among control sensitivity, control bandwidth and disturbance rejection bandwidth using a variable stability helicopter.," in *Proceedings of the 15th European Rotorcraft Forum*, September 12-15 1989.

[5] J. Lusardi, *Control equivalent turbulence input model for the UH-60 helicopter*. PhD thesis, University of California, Davis, Jan. 2004.

[6] S. Seher-Weiss and W. Grünhagen, "Development of ec 135 turbulence models via system identification," *Aerospace Science and Technology - AEROSP SCI TECHNOL*, vol. 23, 12 2012.

[7] S. Seher-Weiß and M. Jones, "Control equivalent turbulence input models for rotorcraft in hover and forward flight," *Journal of Guidance, Control, and Dynamics*, vol. 44, no. 8, pp. 1517–1524, 2021.

[8] O. Juhasz, M. Lopez, M. Berrios, T. Berger, and M. Tischler, "Turbulence modeling of a small quadrotor uas using system identification from flight data," 01 2017.

[9] T. Berger and M. J. S. Lopez, "Frequency domain identification of a multi-input control equivalent turbulence input model," *Journal of Guidance, Control, and Dynamics*, vol. 45, no. 1, pp. 15–27, 2022.

[10] A. G. P. Julius S. Bendat, *Random Data: Analysis and Measurement Procedures*, ch. 5. Wiley, 4th edition ed., 2010.

[11] M. Tischler and R. Remple, *Aircraft and Rotorcraft System Identification: Engineering Methods with Flight Test Examples*. AIAA education series, American Institute of Aeronautics and Astronautics, 2012.

[12] I. Advanced Rotorcraft Technology, *FLIGHT- LAB X-Analysis user manual*. 2013.

[13] M. J. S. Lopez and J. V. R. Prasad, "Linear time invariant approximations of linear time periodic systems," *Journal of the American Helicopter Society*, vol. 62, pp. 1–10, January 2017.

[14] R. G. Lee and S. J. Zan, "Unsteady aerodynamic loading on a helicopter fuselage in a ship airwake," *Journal of the American Helicopter Society*, vol. 49, no. 2, pp. 149–159, 2004.